Available online at www.sciencedirect.com
SCIENCE DIRECT
Polymer 46 (2005) 11773–11785
polymer
www.elsevier.com/locate/polymer

Structural interpretation of the strain-rate, temperature and morphology dependence of the yield stress of injection molded semicrystalline polymers

J.C. Viana *

Department of Polymer Engineering, IPC-Institute for Polymers and Composites, University of Minho, Campus Azurem, 4800-058 Guimarães, Portugal

Received 12 July 2005; received in revised form 27 September 2005; accepted 4 October 2005
Available online 27 October 2005

Abstract

The yield stress of polypropylene specimens with different initial microstructural states is investigated. These latter were obtained by systematic variations of the processing conditions in injection molding, resulting in different laminated skin-core structures. The morphology of the molded specimens was characterized by polarized light microscopy (full specimen), differential scanning microscopy (core layer) and wide-angle X-ray scattering (skin region). The yield stress was evaluated at different nominal strain-rates (1.67×10^{-3} to 150 s^{-1}) and temperatures (23, 40 and 60 °C). The experimental results are analyzed in the frame of Eyring's viscous flow and lamellar cluster models, being established the relationships between the activation volume and enthalpy upon the initial morphological state of the specimens. It is proposed that similar deformation mechanisms operate in both skin and core layers, although with distinct temperature and strain-rate sensitivities. The morphology dependence of the yield stress at different temperatures and strain-rates is established in terms of a laminate composite approach. Yielding is interpreted based on the deformation of crystalline lamellae by the pulling out action of both the molecular chains that are anchored in the inter-lamellar amorphous phase and the tie-molecules. The deformation mechanism operating at the skin and core layers are unified by an elastic-beam mechanical analogue that is able of explaining the morphology, temperature and strain-rate dependences of the yield stress.

Keywords: Yield; Morphology; Deformation mechanism

1. Introduction

Yielding is considered as the onset of irreversible plastic behavior leading to a permanent deformation of the material. The yield point of polymers is dependent upon the temperature and strain-rate, anticipating a strong viscoelastic nature. The experimental observation of the yield point is therefore rendered rather difficult, and a plastic deformation is normally assumed when the strain is not totally recovered (residual or permanent strain) in the same time scale as it was imposed. The yield locus of polymers is also affected by the pressure and by the loading mode (e.g. tensile or compressive) [1].

Macroscopically, yielding is evidenced by the occurrence of a localized necking or the appearance of shear bands. Whitening and crazing may also be observed revealing that some micro-voiding is taking place [2,3] with an increase on the specimen volume. The occurrence of crazing and whitening in polypropylene was found to be dependent upon the temperature and strain rate [2]. These inhomogeneous processes are reflected both on the recorded force–displacement curve, $F-\Delta l$ (which shows a first maximum force value) and/or on the measured true stress–true strain curve, $\sigma_t-\varepsilon_t$ (which evidences an inflection point or, in certain cases, a maximum stress value representing a real strain softening). The definition of the yield point is therefore conventional (e.g. first force maximum, Consideré construction [4], two tangent intersection method, and strain off-set method). These different definitions may apply to the same material under distinct loading conditions (temperature, strain-rate, stress state).

At a molecular scale level, yield in semi-crystalline polymers involves the disruption of the crystalline phase in an irreversible deformation process. Upon yielding, the spherulitic structure is deformed and eventually destroyed and transformed into a fibrillar one as the plastic deformation increases [5]. Apart from the crystalline lamella being broken into small crystalline blocks upon yielding, Liu et al. also observed that the crystalline phase is transformed into amorphous one [6]. Ferreiro and Coulon [7] evidenced the role of the amorphous phase on the plastic deformation at yield of a polyamide 6. Shear bands are developed in the amorphous phase originating crystalline nanoblocks, whose size increases with the strain-rate. Hughes

* Tel.: +351 253 510335; fax: +351 253 510339.
E-mail address: jcv@dep.uminho.pt.

0032-3861/$ - see front matter © 2005 Elsevier Ltd. All rights reserved.
doi:10.1016/j.polymer.2005.10.024

et al. [3] related the onset of both intense micro-voiding and stress-induced martensitic phase transitions (these two phenomena occurring concomitantly) to the yield point. Raults proposed that the yield of semi-crystalline polymers involves some collective chain motions taking place in the crystalline phase (α_c movements) [8]. Nitta et al. explained the yield behavior by the disintegration of lamellar clusters (before deformed by bending due to the action of active tie-molecules) accompanying lamellar fragmentation [9]. The lamellar cluster morphology has observed by TEM for polypropylene, confirming the morphological features proposed by the lamellar cluster theory [10]. Strobl proposed that the deformation behavior of semi-crystalline polymers is strain-controlled rather than stress-controlled [11,12]. The different deformation mechanism taking place under deformation occurs at critical strain points regardless the degree of crystallinity of the samples, the temperature and the strain-rate. The yield point (referenced as point B) is associated to a collective activity of crystallographic slips in the lamellae [13]. Strobl also evidenced the role of the highly entangled amorphous interlamellar zone on the deformation process [11]. Graham et al. found that other factors than the degree of crystallinity strongly affects the yielding behavior of polymers, namely the overall crystallite structure (e.g. lamellar length, curvature, and segmentation) [14].

Several micro-deformation mechanisms of semi-crystalline polymers have been proposed (see reviews in [15,16]). Due to their biphasic nature, some occurs in the crystalline regions (chain and transverse slip by screw and edge dislocations, mechanical twining and stress-induced martensitic phase transformations) and others in the amorphous layer (inter-lamellar shear and separation and lamellar-stack rotation). The crystalline regions are separated by an amorphous network (inter-lamellar region) consisting of dangled chain ends (free ends), chain loops (chain re-entering in the same lamella), floating chains (cilia) and tie-molecules (chains connecting adjacent lamellae). The crystalline lamellae are bridged together by tie-molecules and by a highly entangled amorphous network occasionally anchored in the crystalline lamella, both acting as stress transfer elements. The deformation of both phases is therefore inter-related at some extent. In fact, some of the abovementioned micro-deformation mechanisms occur concomitantly, and they are activated in particular conditions. Generally, the micro-deformation mechanisms of the amorphous phase offer lower resistance than that of the crystalline regions [15,16]. Also, at low strains, the deformation of the amorphous phase is nearly fully reversible upon removal of the load [15].

2. Approaches to yield of semi-crystalline polymers

The yielding of semi-crystalline polymers has been analyzed by different, and sometimes opposed, approaches. It has been considered as a thermal activated rate process described by the Eyring's theory of viscous flow [17–19] that establishes the strain-rate and temperature dependence of yield stress, σ_y. Adopting a crystal plasticity approach, yield was interpreted as the motion of dislocations through the lamellar crystals [20–22]. Yielding has also been looked as a melting-recrystallization phenomena [8,14]. Recently, yield was explained by the deformation of a lamellar cluster [9,10].

2.1. Eyring's theory of viscous flow approach

Yielding has been considered as a thermally activated rate process described by the Eyring's theory [23,24], which considers a molecular model of the flow mechanism. The model assumes that at the yield point $(d\sigma/d\varepsilon)=0$ denoting a momentary condition for viscous flow [2]. This concept was initially developed to model yielding in amorphous materials, but it was also successfully applied to semi-crystalline polymers [1,2,17], evidencing the role of the amorphous phase on the deformation process at yield. However, in this type of polymers the analysis of the deformation mechanism is more complex due to their intrinsic non-homogeneous character. The temperature and strain rate dependence of σ_y is given by:

$$\frac{\sigma_y}{T} = \frac{2}{V^*}\left[\frac{\Delta H}{T} + 2.303R\log_{10}\left(\frac{\dot{\varepsilon}_y}{\dot{\varepsilon}_0}\right)\right] \quad (1)$$

where T is the absolute temperature, V^* and ΔH are the activation volume and enthalpy respectively, $\dot{\varepsilon}_y$ is the strain-rate, $\dot{\varepsilon}_0$ is a constant and R is the gas constant. The Eyring's theory approach has a phenomenological nature. It correlates the effects of the temperature and strain rate on σ_y, but no morphological dependence of σ_y is considered. It predicts a linear dependence of σ_y upon the $\ln(\dot{\varepsilon})$ for a given temperature, if a single mechanism is activated. However, some experimental results show that this linear relationship does not hold for a wide range of temperatures and strain-rates. The Eyring model has therefore been extended to incorporate more than one rate activated process (processes I and II) [2,19]. The Eyring model has also been used combined with a continuum yielding model to predict the yield stress of pressure dependent anisotropic semi-crystalline materials [18].

2.2. Crystal plasticity approach

The yield behavior of semi-crystalline polymers has also been interpreted in terms of crystal plasticity theories [16,21]. Yield is assumed to be due to the thermal activation of screw dislocations within the crystalline lamellae. In these localized motions, the Burgers vector is parallel to the chain axis (c-axis) and the dislocation core radius is proportional to the crystal width. σ_y is expressed as:

$$\sigma_y = \frac{K(T,\dot{\varepsilon})}{2\pi}\exp\left[-\left(\frac{2\pi\Delta G_a(T)}{l_s K(T,\dot{\varepsilon})b_v^2}+1\right)\right] \quad (2)$$

where K is the crystalline shear modulus of the slip planes (temperature and strain-rate dependent), ΔG_a is the Gibbs free energy for nucleation of dislocations (assumed to be proportional to the absolute temperature) and b_v the magnitude of the Burgers vector. This approach allows predicting σ_y from knowledge of the material morphology (stem length, l_s—the length traversed by the polymer chains within a lamella considering that the chain axis is oriented relatively to the lamella surface to a certain angle) for a constant temperature and strain rate. It is applicable when the c-shear (shear along the chain axis, c) is the controlling mechanism for yield,

under conditions of both elasto-plastic (low temperatures) and viscoelastic deformations (high temperatures) [21]. The dependence of σ_y upon the temperature was introduced on the values of K and ΔG_a [21]. Brooks et al. [21] also reported that Eq. (2) cannot model the temperature and stem length dependences in a consistent manner without modifications. Recently, Galeski observed a leveling off on the dependence of σ_y upon the lamella thickness [16], which was attributed to the activation of a different source of dislocations (a Frank–Read source of generation of dislocations). For low lamellar crystal thickness, the screw dislocation travel through the crystal, σ_y being linearly proportional to it. But for higher lamella thicknesses the dislocation line will lock their ends forming a dislocation ring that moves outwards. New rings are continuously being generated, in a mechanism that is independent upon the crystal size [16]. Eq. (2) predicts that σ_y is proportional to the stem length (or better to $e^{(-1/ls)}$). Some authors argued that the dependence to be considered is upon the degree of crystallinity (which is related to the crystal thickness, l_c) [25]. The crystal plasticity dislocation theory predicts the correct order of magnitude of σ_y.

2.3. Melting/re-crystallization phenomena approach

Yielding has also been interpreted as a melting-recrystallization phenomenon. It has been suggested that at the yield point a partial melting of the crystalline phase occurs, which is followed by a thickening process [8,14,26]. These phenomena are able of explaining the systematic differences founded in the shape of yield point (from single, to double and to diffuse yielding) with the degree of crystallinity [27]. Furthermore, the mechanical work for plastic deformation, ΔH_w, compares with the thermal energy of melting, ΔH_m: for polypropylene $\Delta H_w = 193.1$ kJ/mol [2] and $\Delta H_m = 148 - 209$ kJ/mol [28,29]. σ_y was therefore directly related to the lamella thickness, l_c, this meaning that the whole crystalline lamellae are implied during deformation. For polyethylene, an empirical relationship was proposed ($\sigma_y = A + (B/l_c)$, where A and B are material constants [8]). However, this approach does not consider the temperature and strain rate dependence of σ_y.

2.4. Lamellar cluster model

This model considers the lamellar cluster as the central structural entity in the deformation behavior of semi-crystalline polymers [9,10,30]. The lamellar cluster is deformed by bending due to the action of active tie-molecules. At yielding its disintegration occurs, accompanied by the fragmentation of the lamellae. The linear dependence of σ_y upon the tie-molecules fraction was explained by the fact that the increase on the active tie-molecules number reduces the support span of the bending process of the lamellar cluster, this causing the bending stress to fragmentation to increase [9,30]. Considering the theory of elasticity, and assuming that this occurs when a critical value of the elastic strain energy reaches a critical value, U_y, the yield stress is given by:

$$\sigma_y = 2\sqrt{2E_oU_y}\left(\frac{L}{l}\right)^2 = 2\nu\sqrt{2E_oU_y}\Delta F_t = n\sqrt{2E_oU_y} \qquad (3)$$

where E_0 is the modulus of the lamellar cluster, L is the thickness of the lamellar cluster of surface area l^2 (l is, therefore, the distance between adjacent active tie-molecules), ν is the number of chain intertwined in the space (Ll^2) and ΔF_t is the probability of forming an active tie-molecule. This model relates the modulus of elasticity, the stress and energy at yield.

The deformation mechanisms operating in semi-crystalline polymers are complex. Their biphasic nature and structural hierarchy lead to strong amorphous-crystalline interactions and deformations spanning multiple length scales. Generally, the deformation mechanisms work concomitantly in the distinct phases and structural scale levels. This makes rather difficult the identification of the controlling effects and of the governing morphological parameters.

2.5. Morphological dependence of yielding

For a spherulitic microstructure, yield is mainly dependent upon the lamella thickness (or stem length) and on the degree of crystallinity [21,25]. In addition to the degree of crystallinity other structural and morphological factors influence yielding, such as the overall structure of the lamellar crystallites (lamellar length, curvature and segmentation) [14]. Assuming that at yield, more than one rate activated process occurs, the process I is associated with the reconformation of the polymer chains and/or a reduction in lamellar size or perfection without micro-voiding, whereas the process II is characterized by a gross interlamellar separation that produces voids [2]. Brooks et al. [22] pointed out that the stem length dependence of σ_y is related to the most common lamellar species, whereas the temperature dependence is associated with the thinner lamellae (stem length of the order of 25–20% of the most common species). Furthermore, Brooks et al. also proposed that the yield stress is also influenced by the lamellar fold surface morphology. This may occur by changes on the nucleation energy to form a screw dislocation within the crystalline lamellae or on the coefficient of friction of the fold surfaces affecting the interlamellar shear [31]. A linear relationship between σ_y and the tie-molecules fraction was experimentally observed for PP copolymers [9]. The contribution of these entities as load transmitters was emphasized, being proposed that a lamellar cluster is central structural unit [10]. Nitta and Yamamoto investigated the mechanical behavior of transcrystalline PP, suggesting that the yielding process is basically governed by the supramolecular structure (spherulitic and transcrystalline morphologies, amount of cross-hatching) and not by the degree of crystallinity [32]. Strobl et al. proposed a common deformation scheme followed by semi-crystalline polymers [13,33] that is controlled by the strain rather than by the stress. While the stress varies significantly as the structure evolves during the deformation process (increasing with the increment on the degree of crystallinity), the strain at which these structural changes occur are invariant regardless the degree of crystallinity of the material [12,13]. The yield stress (and modulus) of syndiotatic PP has found to change only slightly with the crystal thickness, being mainly controlled by the block-like substructure of the lamellar crystallites [13].

Using computer simulations of the deformation behavior of a lamellar structure, Viana et al. identified the thickness of the crystalline lamellae and the mechanical behavior of the amorphous phase as the most significant factors affecting the yield response of semi-crystalline polymers [34].

3. Yield of injection molded semi-crystalline polymers

3.1. Structure development in injection molding

An injection molded semi-crystalline polymer shows a heterogeneous and hierarchical structure [35–38]. This morphology is developed upon the constrains imposed by the thermomechanical environment applied to the polymer during the processing stages [38]. At a microscopic level (optical microscope resolution) a typical laminated skin-core microstructure is observed (Fig. 1).

In the skin layer the molecular chains are highly oriented in the flow direction due to the high strain-rates and rapid cooling imposed during processing. These chains are highly extended forming central bundles (shishes) in which radial lamellae grow epitaxially (kebabs). By analogy, these crystalline forms are referred to shish–kebab structures (Fig. 1). The core region is composed of spherulite-like structures due to the very low (or even the absence) of shear deformation and the slower cooling rates. In between the skin and core layers a transition zone may be discriminated. The relative dimensions of these layers (skin ratio—the quotient between the skin and the total specimen thicknesses) and their morphological state (e.g. spherulite size, lamella thickness, degree of crystallinity, level of molecular orientation) are dictated by the highly coupled thermal and mechanical conditions applied during processing [38–40]. These conditions are determined by the setting of the operative variables (e.g. melt and mould temperatures, injection flow rate, holding pressure), by the molding geometry (e.g. thickness, maximum flow length, gating options) and the material properties (e.g. physical and rheological). The processing induced morphology of semicrystalline polymers is highly heterogeneous and markedly determines the mechanical behavior of the molded materials.

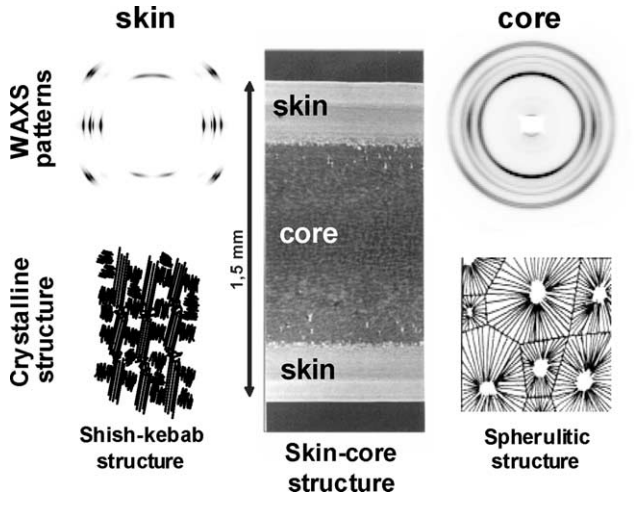

Fig. 1. Microstructure of an injection molded semi-crystalline polymer: centre-skin-core structure as observed by polarized light microscopy; left—WAXS pattern of the skin layer and correspondent crystalline structure; right—WAXS pattern of the core layer and correspondent crystalline structure.

3.2. Processing-morphology-yield properties relationships in injection molding

σ_y of injection molded PP specimens is dependent upon the morphological features of the skin-core structure. Considering a laminate approach, σ_y was related to the skin ratio [35,40,41] and to its high level of molecular orientation [41,42]. Schrauwen et al. interprets the enhancement of σ_y with the level of molecular orientation by the formation of extended crystals [42]. σ_y of highly oriented specimens produced by non-conventional injection molding techniques (SCORIM) was found to be superior to conventional ones. This was attributed to the increment on the thickness of the highly (multi-laminated) oriented skin layer and its high level of molecular orientation [43]. σ_y of injection molded sample was in addition connected to the degree of crystallinity of the core region, considering its spherulitic crystalline structure [41]. σ_y of injection molded specimens was also linked to other morphological parameters such as the spherulite type and crystal forms [44].

3.3. Work description

σ_y of an injection molded PP copolymer was assessed at different strain-rates and temperatures for specimens molded with different processing conditions (inducing distinct initial morphological states). The relationships between the processing induced morphology and σ_y are established for the distinct temperatures and strain rates. The results are discussed in the light of the Eyring and lamellar cluster models and their dependence upon the morphological parameters. Finally, an interpretation of the strain-rate, temperature and morphology dependence of σ_y is given based in a structural model.

4. Experimental

4.1. Material and molding

Axi-symmetric dumbbell tensile specimens (1.5 mm of diameter and 20 mm of reference length) were injection molded in a polypropylene copolymer (Appryl 3120 MR5) with variations of the processing conditions (Table 1).

Table 1
Injection molding processing conditions

Ref.	T_{inj} (°C)	T_w (°C)	Q_{inj} (cm^3/s)
200/30/10	200	30	10
230/5/10	230	5	10
230/30/40	230	30	40
230/30/10	230	30	10
230/30/5	230	30	5
230/80/10	230	80	10
270/30/10	270	30	10

T_{inj}, melt temperature; T_w, mould temperature; Q_{inj}, injection flow rate.

Table 2
Structural characterization of the injection molded specimens

Ref.	Sa	χ_s	Ω_s	χ_c	l_c (nm)	ΔH (J/kg)	l_{ave} (nm)
200/30/10	0.494	0.503	0.871	0.507	17.8	73.51	17.9
230/5/10	0.356	0.379	0.835	0.487	17.7	80.44	17.7
230/30/40	0.223	0.449	0.867	0.501	18.1	75.23	17.5
230/30/10	0.331	0.460	0.800	0.494	17.8	80.16	17.5
230/30/5	0.438	0.472	0.853	0.519	17.7	80.11	17.6
230/80/10	0.318	0.474	0.758	0.518	18.3	81.84	17.3
270/30/10	0.268	0.434	0.725	0.494	18.2	79.88	17.6
Δ (%)	121.5	32.7	20.1	6.6	3.2	11.3	2.9

Sa, skin ratio; χ_s, degree of crystallinity of the skin; Ω_s, crystalline phase orientation index of the skin; χ_c, degree of crystallinity of the core; l_c, thickness of core lamella; ΔH, average enthalpy of melting of the molding; l_{ave}, average lamella thickness of the molding; Δ, percentage variation of the morphological parameter = [max − min]/min.

4.2. Morphological characterization

The molded specimens show a heterogeneous structure that has been characterized by different experimental techniques:

- Polarized light optical microscopy, PLOM, to measure the thicknesses of the layered microstructure (evaluated by the skin ratio, Sa).
- Differential scanning calorimetry, DSC, only of the core layer allowing the assessment of the degree of crystallinity, χ_c, and lamella thicknesses, l_c, of the core.
- Wide-angle X-ray scattering, WAXS, of the skin layer alone, which allows evaluating its level of crystalline phase orientation, Ω_s, and its relative degree of crystallinity, χ_s.

Details on these techniques and on the relationships between the processing thermomechanical environment and the microstructure development can be found elsewhere [38]. The Table 2 summarizes the results of the structural characterization.

4.3. Mechanical testing

The mechanical behavior of the moldings was assessed at different temperatures (23, 40 and 60 °C at 2 mm/min) and strain-rates (2, 10, 100 and 500 mm/min and 3 m/s at 23 °C; corresponding to nominal strain-rates of 1.67×10^{-3}, 8.33×10^{-3}, 8.33×10^{-2}, 4.17×10^{-1} and 150 s^{-1}, respectively). The test conditions were varied as shown in Table 3.

The yield point was defined as the first maximum in the force–displacement curves (F_y and Δl_y, the force and displacement at the yield point, respectively). The homogeneous yield stress, σ_y, was calculated.

Table 3
Test conditions of the tensile experiments

T (°C)	V (m/s)/(mm/min)	$\dot{\varepsilon}$ (s^{-1})
23	3.33×10^{-5}/2	1.67×10^{-3}
40	3.33×10^{-5}/2	1.67×10^{-3}
60	3.33×10^{-5}/2	1.67×10^{-3}
23	1.67×10^{-4}/10	8.35×10^{-3}
23	1.67×10^{-3}/100	8.35×10^{-2}
23	8.333×10^{-3}/500	4.17×10^{-1}
23	3/1.80×10^{5}	1.50×10^{2}

T, test temperature; v, test velocity; $\dot{\varepsilon}$, nominal strain-rate.

5. Results and discussion

The $F-\Delta l$ curves obtained at different test velocities for specimens molded with extreme values of the melt temperature are presented in Fig. 2.

In all the curves a first force maximum is observed, which significantly increases with the strain rate. At higher melt temperature (T_{inj} = 270 °C) yield occurs for lower force value and the deformation capabilities of the moldings are higher. As the strain-rate increases, the force drop becomes narrower indicating the more localized nature of the neck formation. Fig. 3 depicts the general effect of processing on the yield stress: σ_y increases with decreasing melt temperature and flow rate and with the increment on the mould temperature.

These dependences are higher upon T_{inj}, which has been found to be the most significant processing variable affecting the structure development in injection molding [36,38]. However, the direct link between the processing variables and the mechanical properties is not a satisfactory route and it will not be discussed further.

5.1. Temperature and strain-rate dependences of σ_y

The effect of the strain rate on σ_y is presented in Fig. 4 for samples molded with different melt temperatures. A linear dependence of σ_y on $\log(\dot{\varepsilon})$ is observed with a slope slightly decreasing with the increment of the melt temperature. On the range of strain rates considered, it may be assumed that σ_y varies linearly with $\log(\dot{\varepsilon})$ as described by Eq. (1), suggesting that a single rate mechanism is activated.

Fig. 5 shows the variations of σ_y with the test temperature. In the selected temperature range, σ_y decreases linearly with the increment of the test temperature with a slope slightly decreasing for the highest melt temperature.

The morphology of injection moldings may be substantially changed by variations on T_{inj} [36,38]. From Table 2, varying T_{inj} from 200 to 270 °C reduces the skin layer thickness in 84%, its level of molecular orientation in 20.1% and its degree of crystallinity on 15.8%, whereas the degree of crystallinity and the lamella thicknesses of the core remains practically constants (2.7 and 2.0%, respectively). These changes on the morphology are translated into variations on the magnitude of σ_y. Furthermore, the dependences shown in Figs. 4 and 5

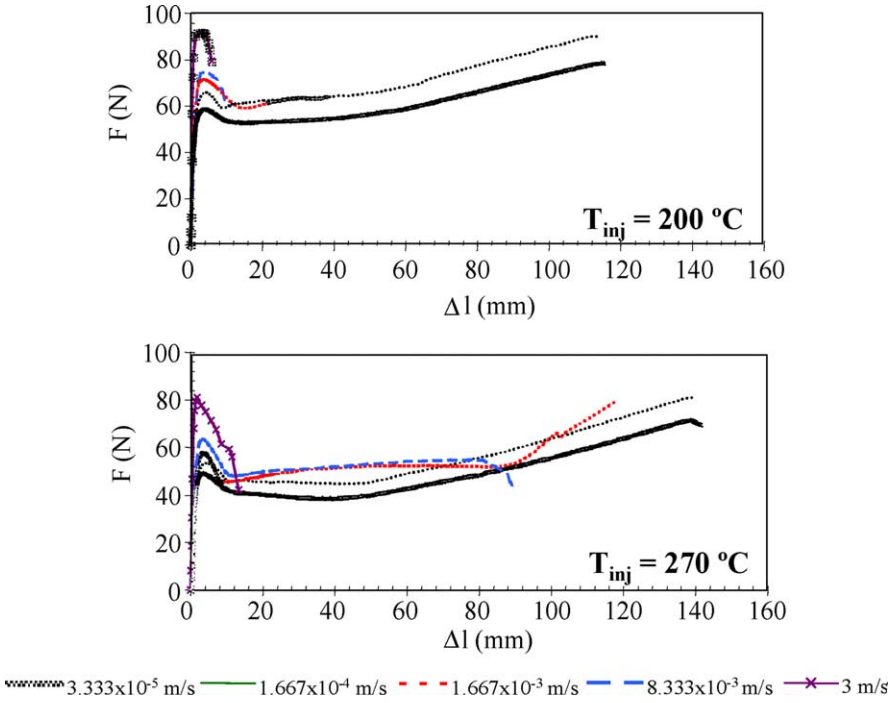

Fig. 2. Effect of the test velocity on the stress–strain curves for specimens molded with extreme melt temperatures of 200 and 270 °C.

suggest that similar deformation mechanisms are activated, in spite of the different and highly heterogeneous microstructures of the moldings. The temperature and strain-rates dependences of σ_y are also slightly influenced by the microstructural differences of the mouldings.

5.2. Molecular approach to yield

The dependences of σ_y on $\log(\dot{\varepsilon})$ and on the test temperature shown in Figs. 4 and 5, respectively, may be described by the Eyring model, assuming a single rate activated process (Eq. (1)). Fig. 6 shows the variation of V^* with the morphological parameters, namely, the degree of crystallinity of skin and core layers and the skin ratio, respectively χ_s, χ_c and Sa.

It is assumed that the relative effect of χ_s and χ_c can be weighted by the thickness of the skin (Sa) and core (1 − Sa) layers, respectively. Furthermore, it is considered that two flow mechanisms operate, one in the skin and another in the core layer, both contributing for the total activation volume. The fitting plane to the experimental data of Fig. 6 can be assumed as good ($R^2 = 0.79$ and a maximum residual of 4.8%). V^* increases with the decrement of χ_s and χ_c, which may be related to a more global amorphous state of the material, and hence to a higher molecular mobility. Both degrees of crystallinity of the skin and core contribute almost equally to the variations on V^*, presaging the existence of similar deformation mechanisms on both crystalline structures. V^* has found to sigmoidally decrease with increased degree of crystallinity of melt-spun PET filaments [45]. The dependences shown in Fig. 6 suggest the high contribution of the amorphous phase to V^*. The strain-rate sensitivity index is related to the activation volume, V^*,

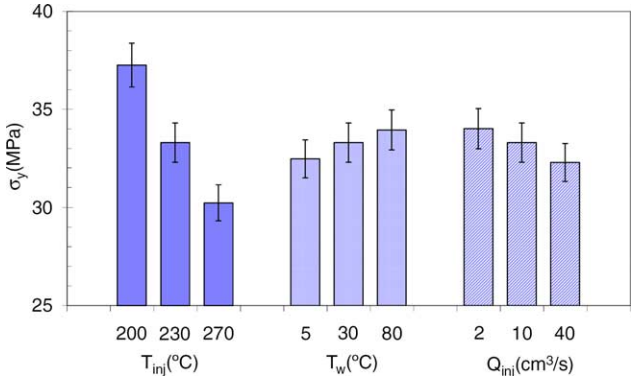

Fig. 3. Dependence of the yield stress, σ_y, upon the melt and mould temperature, T_{inj} and T_w, and flow rate, Q_{inj} (test velocity and temperature of 2 mm/min and 23 °C, respectively).

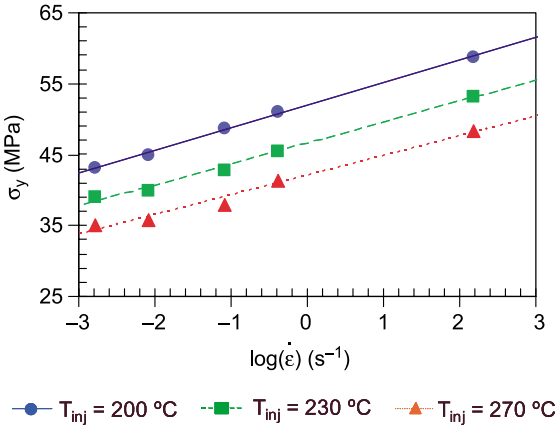

Fig. 4. Effect of the strain rate, $\dot{\varepsilon}$, on the yield stress, σ_y, at test temperature of 23 °C for different melt temperatures (constant $T_w = 30$ °C and $Q_{inj} = 10$ cm^3/s) (coefficient of linear regression of $R^2 = 0.998$, 0.998 and 0.986 for $T_{inj} = 200$, 230 and 270 °C, respectively).

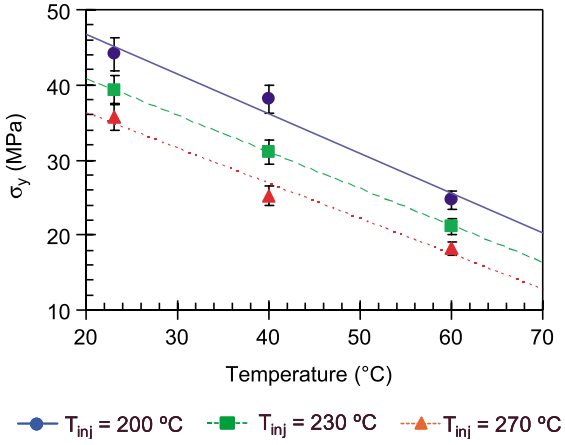

Fig. 5. Effect of the test temperature, T on the yield stress, σ_y, at test velocity of 2 mm/min for different melt temperatures (T_w = 30 °C and Q_{inj} = 10 cm^3/s) (coefficient of linear regression of R^2 = 0.97, 1.00 and 0.97, respectively, for T_{inj} = 200, 230 and 270 °C).

assuming a single activated process [23]. This presages a stronger strain-rate dependence of the core layer than the skin.

Fig. 7 shows the variation of ΔH as a function of the morphological parameters, namely, the level of crystalline phase orientation, the core lamella thickness and skin ratio, respectively Ω_s, l_c and Sa. ΔH is related to the difficulty of the flow unities in overpass the energetic barrier (to flow) from two equilibrium states, so to the strength of the transition. It is assumed that Ω_s and l_c are the main morphological parameters of the skin and core layers, respectively, contributing for the total ΔH.

ΔH increases markedly with SaΩ_s. It also increases, in a lower extent, with (1 − Sa) l_c. Both the level and amount of molecular orientation and the lamella thickness contribute to ΔH, suggesting the importance of the crystalline phase on σ_y. ΔH was found to linearly increase with the increase on the degree of crystallinity of melt-spun PET filaments [45]. It was suggested that the yield process occurs in the amorphous regions, the crystals acting as flow obstacles, so increasing the energy barrier for yielding. However, the level of orientation of the PET samples was also concomitantly incremented and both effects could not be separated.

Although, the Eyring model has been used to model the yield process in semicrystalline polymers, a molecular

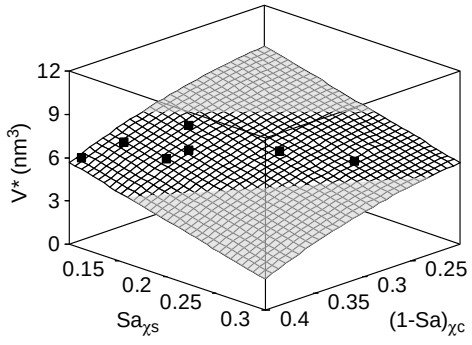

Fig. 6. Variation of the activation volume, V^*, with the skin ratio weighed skin and core degree of crystallinities, χ_s and χ_c, respectively (R^2 = 0.79, maximum residual of 4.8%).

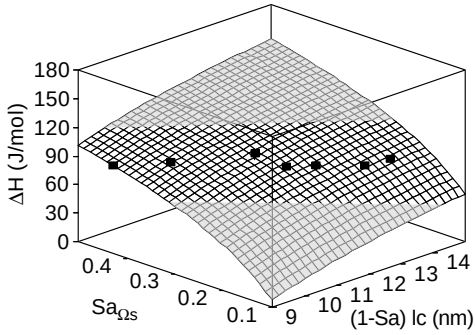

Fig. 7. Variation of the activation enthalpy, ΔH, with the skin ratio weighed level of orientation of the skin, Ω_s, and lamella thickness of the core, l_c (R^2 = 0.67; maximum residual of 6.3%).

interpretation has not been given yet. From the results of Figs. 6 and 7, two flow processes are activated at yield in the skin and core layers, although involving similar deformation mechanisms. Both the skin and core layers comprise crystalline and amorphous phases. In each phase different flow mechanism can operate. In the amorphous regions, the flow process is characterized by a high V^* and low ΔH, whereas in the crystalline phase, the flow mechanism is oppositely operated with a low V^* and high ΔH. Upon yielding, the higher contribution to V^* will come from the amorphous phase, while to ΔH it will arise from the crystalline regions. The similar morphologies of the amorphous phase of both skin and core layers equally contribute to the overall V^* (Fig. 6). On the other hand, the different crystalline structures of both these layers will presage different contributions to the total ΔH.

5.3. Lamellar cluster model approach

Accordingly to Eq. (3), there should be a direct linear relationship between σ_y and $\sqrt{2EU_y}$ regardless the test temperature and strain-rate. Fig. 8 shows such a plot for specimens molded with the two extreme injection melt temperatures.

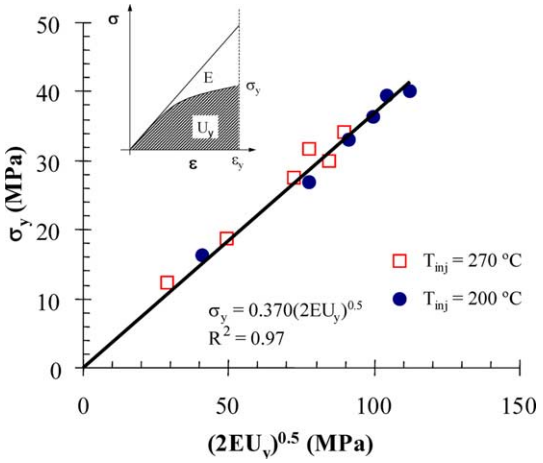

Fig. 8. Variation of the yield stress, σ_y, with the initial modulus, E, and the energy at yield, U_y, according to Eq. (3) for specimens molded with different melt temperatures, T_{inj}, of 200 and 270 °C.

In spite of the distinct morphological states of the specimens molded with different melt temperatures (Table 2) all the data falls in a straight line given by $\sigma_y = 0.370\sqrt{2EU_y}$ (with a coefficient of linear correlation of $R^2 = 0.97$). This may be an evidence of similar deformation mechanisms operating independently of the temperature, strain-rate and morphology of the specimens. Nitta et al. found a value for the same slope of $n = 0.33$ for an isotatic PP [9]. The values of n are surprisingly closer, considering the different morphologies of their compressed (iPP) and our injection molded (PP copolymer) specimens. Again, the operating deformation mechanism should be identical in both compressed and injection molded specimens. Furthermore, n can be looked as an indication of the deviation from a purely linear behavior (characterized by $n = 1$; see inserted graph in Fig. 8). Its morphological dependence should be better verified.

5.4. Crystal plasticity and melting/re-crystallization phenomena approaches

Table 2 also shows the results of DSC of total molded samples (considering the skin and core layers), being listed the average enthalpies of melting and lamella thicknesses of the different moldings. No apparent correlations could be established between σ_y at distinct strain-rates and the lamella thickness (crystal plasticity approach) and the values of σ_y and the enthalpies of melting (melting/re-crystallization approach). These may indicate that these types of relationships should be established locally (e.g. for the skin and core layers separately, i.e. for shish–kebab and spherulitic structures individually) and they cannot be simply averaged. Furthermore, other morphological parameters may also be considered.

5.5. Morphological dependence of σ_y in injection molding

5.5.1. Laminate model approach

Simplified laminated models and the classical composite theory have been used for establishing relationships between the morphology and the mechanical properties in injection molding [46,47]. In fact, one can consider a three layer configuration (skin-core) in which σ_y is mainly dictated by two morphological parameters (assumed as the most significant; this approach was already previously adopted in Figs. 6 and 7): the level of crystalline phase orientation of the skin, Ω_s, and the core lamella thickness, l_c. In an uniaxial loading this can be expressed as:

$$\sigma_y = a\mathrm{Sa}\Omega_s + b(1-\mathrm{Sa})l_c \quad (4)$$

where Sa is the skin ratio, a and b are fitted coefficients. These dependences are shown in the Fig. 9 that presents the trends of variation of σ_y upon the microstructure for the different test velocities.

σ_y increases with both skin ratio weighted morphological parameters, being more dependent upon the initial level of orientation of the moldings. The strain-rate sensitivity of σ_y is slightly higher for thicker and more oriented skin layers (highest values of $[\mathrm{Sa}_s]$) and for thinner core layers with thicker lamellae (highest values of $[(1-\mathrm{Sa})l_c]$).

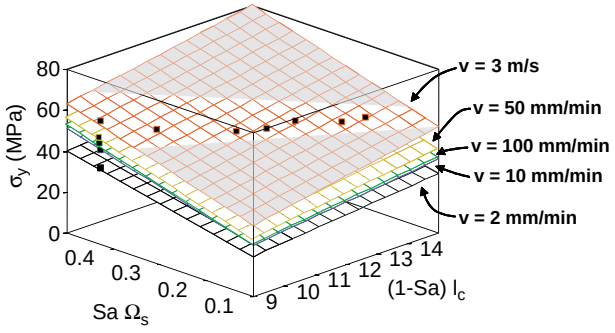

Fig. 9. Effect of the test velocity on σ_y at test temperature of 23 °C for the different molded specimens (Sa—skin ratio, Ω_s—level of crystalline phase orientation of the skin layer, l_c—thickness of the core lamella). The experimental points were fit with Eq. (4).

The quality of the model fittings, evaluated by the coefficient of multiple regression, R^2, is of 0.79, 0.80, 0.75, 0.77, 0.78, 0.78 and 0.55, respectively from the lowest to the highest test velocities. Eq. (4) describes fairly well the experimental data, except at highest test velocity where R^2 is significantly smaller. This may be attributed to the higher experimental error, but also to a less goodness of the fitted model. Nevertheless, other morphological parameters should be considered in order to improve the correlations. This also points out for the need of a better physical understanding of the morphological changes occurring at yield, so that physically based models could be developed. In this work, the polynomial model of Eq. (4) was selected (although not totally arbitrarily) to allow comparing the strain-rate and temperature dependences upon the molding microstructure.

The dependences of σ_y upon the test temperature also reveal different morphological sensitivities, as shown in Fig. 10. This is mainly evidenced by the distinct slopes of the variations of σ_y with $\mathrm{Sa}\Omega_s$ at different temperatures. The temperature sensitivity of σ_y is higher for thicker and more oriented skin layers.

The quality of the model fittings (again evaluated by R^2) is of 0.75, 0.80 and 0.74, respectively, for the test temperatures of

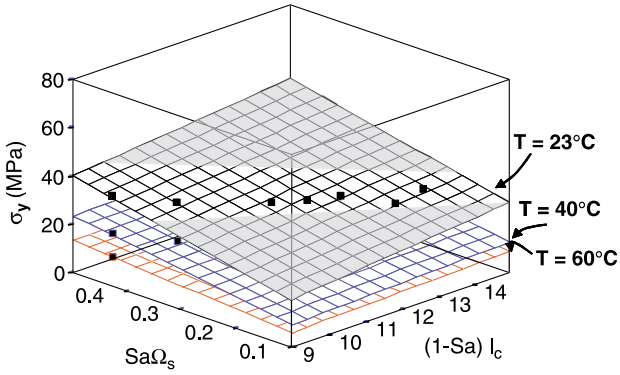

Fig. 10. Effect of the test temperature on the σ_y at velocity of 2 mm/min for the different molded specimens (Sa—skin ratio, Ω_s—level of crystalline phase orientation of the skin layer, l_c thickness of the core lamella). The experimental points were fit with Eq. (4).

23, 40 and 60 °C. Eq. (4) also describes fairly well, the experimental data, but again, other morphological parameters should be considered in order to improve the correlations, as already abovementioned.

In Figs. 6–10, the location of the experimental points in a narrow strip along the fit plane is a consequence of the strong coupling between the thermal and mechanical levels imposed to the polymer during processing [38,41]. The dispersion of these points may be enlarged by changing the material properties [47,48] (e.g. its rheological behavior and crystallization kinetics) and/or by using non-conventional melt manipulation injection molding techniques (e.g. SCORIM and PUSH–PULL) [4,49].

The use of Eq. (4) as a fit polynomial expression allows the calculation of the coefficients a and b, which represents the relative importance of each morphological feature on the values of σ_y. In order to avoid scale effects, the values of the level of crystalline-phase molecular orientation of the skin (Ω_s) and the core lamella thickness (l_c) were normalized with respect to their maximum values. The variations of these fitted coefficients with the test strain-rate and temperature are shown in the Figs. 11 and 12, respectively. The dependence of a (skin layer coefficient) upon the test strain-rate (Fig. 11) rapidly reaches a plateau value, suggesting a saturation of the effect of the skin layer.

The coefficient b (core layer) also increases almost linearly with the strain-rate. It seems that the influence of the core becomes more significant as the strain-rate increases. This higher strain-rate sensitivity of the core was already abovementioned. The mechanical properties of the moldings at high strain-rates are basically controlled by the skin layer characteristics [50], but its strain rate sensitivity is lower. These trends are inverted when the dependences on the test temperature are considered (Fig. 12). In this case, the effect of the core layer tends for a plateau value as the test temperature increases, and the contribution of the skin layer is gradually reduced. It appears that the influence of the core becomes less important as the test temperature increases, that is, its shows less temperature sensitivity. Nevertheless, the contribution of the skin layer is still more significant for the yield stress.

In fact, the relative importance of the skin layer on σ_y is higher in the considered experimental window, as

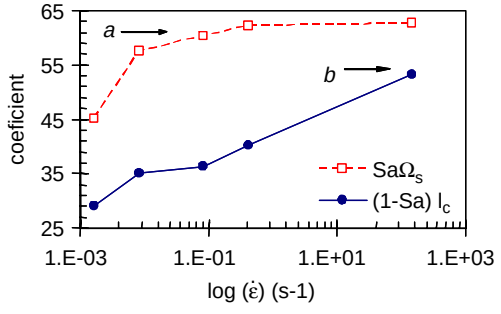

Fig. 11. Variations of the model coefficients of Eq. 4, corresponding to the morphological parameters $Sa\Omega_s$ and $(1-Sa)l_c$, with the logarithmic strain rate (the morphological parameters were normalized between 0 and 1 to avoid scale effects).

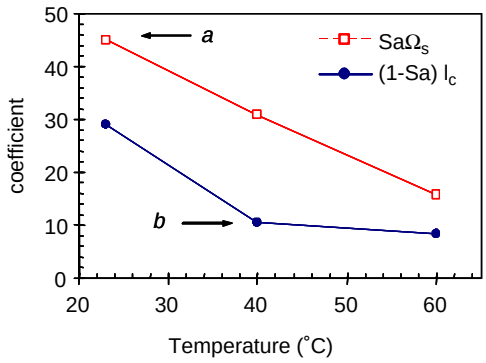

Fig. 12. Variations of the model coefficients of Eq. 4, corresponding to the morphological parameters $Sa\Omega_s$ and $(1-Sa)l_c$, with the test temperature (the morphological parameters were normalized between 0 and 1 to avoid scale effects).

the coefficients a are always higher than the b ones. Furthermore, as the strain-rate and temperatures increase, the differences between both skin and core layers contributions are attenuated. Nevertheless, the skin layer shows a lower strain rate but higher temperature sensitivities than the core region. This behavior is depicted in Fig. 13 that shows the expected stress distributions on the skin and core layers.

It is assumed a heterogeneous skin-core structure, which due to their distinct morphological states, differently reacts the imposed strain field, originating a non-uniform stress distribution through the molding cross-section. Fujiyama measured the stress–strain curves of the skin and core layers of injection moldings [36]. For the particular morphological states, the skin

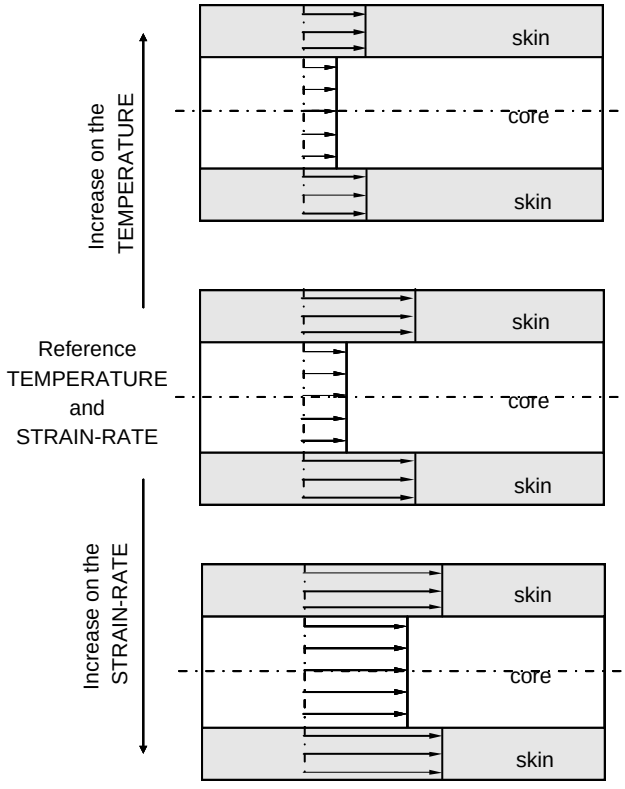

Fig. 13. Effect of increasing strain-rate and test temperature on the stress distribution in the skin and core layers of an injection molding.

showed a significant higher modulus and yield stress than the core layer, but this later had a higher deformation capability, due to its low level of molecular orientation. The strain-rate and temperature sensitivities of both layers were not assessed. Nevertheless, at higher strain-rates and temperatures, the skin-core stress distribution is more homogeneous due to the distinct strain-rate and temperature sensitivities of the skin and core morphologies, as above referred to. In spite of these distinct strain-rate and temperature sensitivities, the average yield stress increases linearly with the $\log(\dot{\varepsilon})$ (Fig. 4) and decreases linearly with the temperature (Fig. 5), as in a simple rate activated behavior. This may evidence that similar deformation mechanisms operate in both skin and core layers that are activated as a response of their distinct morphological states.

5.5.2. Deformation mechanisms in the skin and core layers

Both shish–kebabs and spherulites crystalline arrangements are composed by chain folded lamellae. In a spherulite, the lamellae grow radially forming the arms of the crystalline structure. For the particular case of polypropylene, in its crystallographic α-form, a crystalline network is formed consisting of radial dominant lamella in which growth epitaxially subsidiary lamella forming a cross-hatched structure [36]. In a shish–kebab structure, the dominant lamellae grow epitaxially in the fibrous central nucleus. Subsidiary lamella growth epitaxially on these kebabs, also forming a crystalline network structure. When the polymer is stretched, the amorphous phases deforms easily due to their enhanced molecular mobility. The crystalline lamellae are deformed by the pulling out action of molecular chains that are anchored in the inter-lamellar amorphous phase and of tie-molecules. Both crystalline structures (spherulites and shish–kebabs) will have therefore distinct deformation constrains (Fig. 14):

- the lamellae in the spherulite (mainly in its equatorial zone) are more prone to a flexural state (transversal loading) [30,51], due to the relative high span between pulling points, L, allowing for a higher flexibility of the lamellar structure.
- Whereas, in the shish – kebab structure, the lamellae are more subjected to a shear loading owning to their reduced size (closest packing), leading to lower L and reduced flexibility capabilities.

In both cases, the yield point corresponds to the disruption of the lamella continuity, by shearing of a lamellar molecular segment along a preferential crystallographic plane when a critical shear stress level is achieved. A similar deformation mechanism operates in both skin and core layers as already above suggested. In the case of a shish kebab structure, a higher force is required to disrupt a lamella due to the applied boundary conditions. This explains the higher yield stress of the skin layer.

5.5.3. Elastic mechanical analogue

Let us consider a continuous mechanical analogue, and assume a lamellar structure as an elastic beam, as in a lamellar cluster model [9,10,30] (this idealization may also be applied to a block-like lamellar structure as proposed by Strobl et al. [52]). The cross-section is $l_c w$, where l_c and w are the lamella thickness and width, respectively. Let also assumes two main types of loadings:

- shear (for high l_c/L ratio),
- flexural (for low l_c/L ratio).

The shear force acting along the lamella cross-section, F_s, is given by:

$$F_s = l_c w \tau \tag{5}$$

where τ is the shear stress. In a flexural loading, the bending force, F_f, is calculated by:

$$F_f = \frac{l_c^2 w \sigma}{\alpha L} = \frac{2 l_c^2 w \tau}{\alpha L} \tag{6}$$

where α is a factor depending on the boundary conditions of the loading (for a simply supported beam between a span of L, $\alpha = 1.5$). If a critical shear stress is assumed to induce in both cases a crystallographic slip motion, $\tau = \tau_c$, the following relationship between F_s and F_f is obtained (substituting (5) in (6)):

$$F_f = \frac{2 l_c F_s}{\alpha L} \quad \text{or} \quad \frac{F_s}{F_f} = \frac{\alpha L}{2 l_c} \tag{7}$$

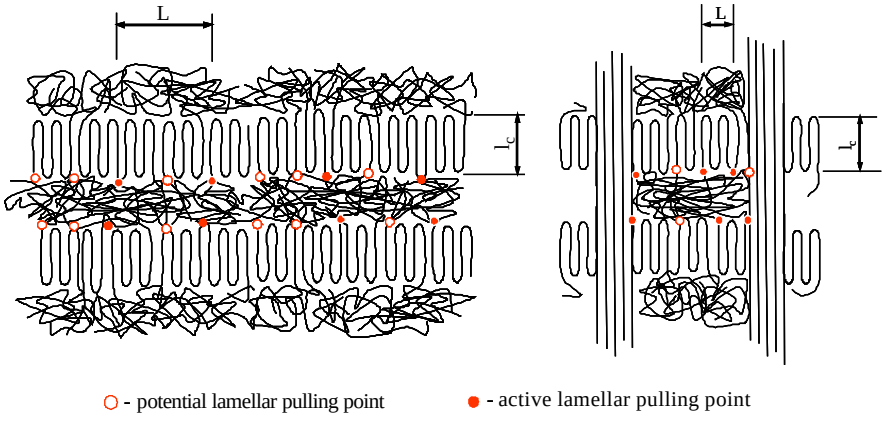

Fig. 14. Representation of the shish–kebab and spherulitic crystalline structures, indicating potential and active lamellar pulling points (not to the scale).

Nitta, assuming the lamellar cluster model, estimated a value of $L=240$ nm and a lamellar cluster thickness, l_c^*, of 98 nm for iPP [9], giving a $F_s/F_f=1.84$. In our case $l_c \approx 18$ nm in the core region, leading to $F_s/F_f=10$. This means that, in the spherulitic inner core, the critical shear stress will be reached in the bending mode. Similarly, the shear forces will become important ($F_s/F_f>1$) for $L/l_c<1.33$. It is expected that the L will be small in a shish–kebab crystalline structure, and so the preponderant deformation mechanism will be by shear.

As shown in Figs. 9 and 10, the yield stress is related to the level of orientation of the skin layer. This effect can be introduced in Eq. (5) considering that the force shear, F_s', to deform a lamella is reduced as the level of crystalline phase orientation is lower, that is:

$$F_s' = F_s \cos(\theta) = l_c w \tau_c \cos(\theta) \tag{8}$$

where θ is the angle between the applied force and the shish–kebab main orientation direction. If $\theta=0$ then $F_s'=F_s$ else $F_s'<F_s$. However, this assumes that the main deformation mechanism of a shish–kebab structure is by shear. This needs to be validated by assessing the dimensions of this crystalline structure and the correspondent effect of the processing conditions.

Let consider now the distinct strain-rate and temperature sensitivities of both different skin and core crystalline structures. When a semi-crystalline polymer is stretched the amorphous phase acts as a stress transfer element, applying the load on the lamellae through lamellar pulling points (marked circles in Figs. 14 and 15(a)). This develops a stress state in the crystalline region causing its deformation. The lamellar structure is supposed to have a potential number of pulling points, obviously depending on the crystallization conditions (Fig. 15(a)). However, only part of these potential points is activated when the stress is transferred to the crystalline lamella through the amorphous region (filled circles in Figs. 14 and 15(b)). This may be related to the activation of entangled molecular regions in the amorphous phase that trigger the potential pulling points that become active. The highest the strain-rate or the lowest is the temperature, the higher is the number of activated lamellar pulling points so that the deformation capabilities of the lamella are reduced resulting in a higher yield stress. This activation of pulling points may occur between the same adjacent lamellae reducing the lamellar deformation span, L (Fig. 15(c)) or in different adjacent ones originating a thicker lamellar cluster (Fig. 15(d)).

A spherulite structure should have a higher number of potential pulling points due to the higher length of the lamella comprising the spherulite radial arms. This, by itself, results in a high strain-rate and low temperature sensitivity of spherulites compared to the shish–kebab structures. Furthermore, the concomitant dependence of F_f upon L and l_c (or l_c^*, the thickness of a lamellar cluster) makes it more sensitive to the strain-rate, as expected. Conversely, the amorphous phase filling the shish–kebab crystalline skeleton may have a reduced number of lamellar pulling points and so only slightly affecting the boundary conditions during lamellar deformation. Moreover, and accordingly to Eq. (8), a shear force is independent upon L,

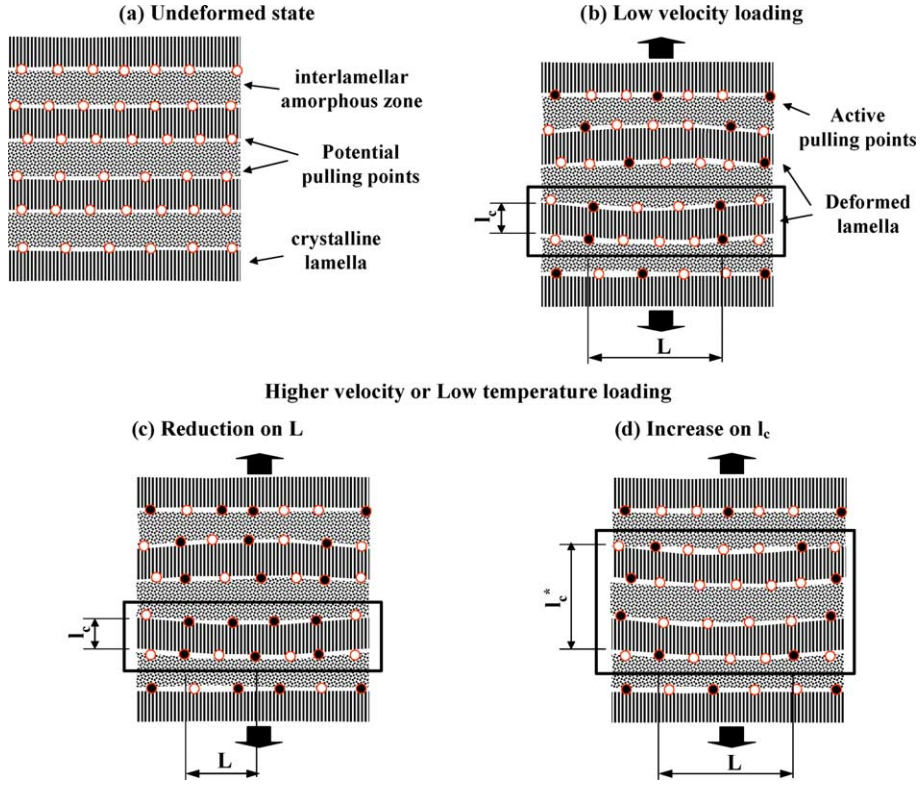

Fig. 15. Activation of lamella deformation by lamellar pulling points due to the action of the amorphous phase. Effect of temperature and strain-rate on the deformation mechanisms of a lamellar cluster.

i.e. to distance between lamellar pulling points. This results in a lower strain-rate sensitivity of the skin layers, as abovementioned.

The variations on the temperature have a double effect. An increment of the temperature will decrease the critical shear stress for crystallographic slip, τ_c, reducing the sustained force levels. This effect is similar for both loading cases (Eqs. 6 and 8). On the other hand, L will increase and/or l_c^* will be decremented with increased temperature, due to a high mobility of the amorphous phase incurring in a lower activation of entangled regions. This will reduce more substantially and drastically the values of F_f and the core becomes rapidly less sensitivity to changes on the temperature. On the other hand, assuming a predominant shear deformation of lamellae in the shish–kebab structure, F_s is mainly dependent upon τ_c that decreases with the temperature (Fig. 12).

6. Conclusions

In spite of the complex morphology featured by injection molded samples of polypropylene (PP), the temperature and strain-rate variations of σ_y present simple dependences as in the case of isotropic spherulitic material. This anticipates that similar deformation mechanisms operate in both skin and core layers, although with distinct temperature and strain-rate sensitivities.

The relationships between the morphology and σ_y of an injection molded PP were established. This was based on a simple laminate composite model that applies to the behavior at different strain-rates and test temperatures. σ_y increases with the thickness and level of crystalline phase orientation of the skin layer and the thickness of the core lamella. Both the skin and core layers distinctly contribute for the variations of σ_y with the strain-rate and temperature. The dependence of σ_y upon the morphology is higher for higher strain-rates and lower test temperatures. As the strain-rate increases the contribution of the morphological parameters of the skin layer saturates and the effect of the core layer becomes more pronounced. Conversely, the role of the core layer stagnates and the importance of the skin layer becomes more important with increments on the test temperature. Seemingly, the core layer is more sensitive to the strain-rate rather than the skin layer, whereas this latter is more sensitive to the temperature than the former.

The effect of strain and temperature on the yield stress is interpreted in terms of the morphology response to the applied loading. Yielding is interpreted based on the deformation of crystalline lamellae by the pulling out actions of molecular chains that are anchored in the inter-lamellar amorphous phase and of tie-molecules. A potential number of lamellar pulling points (LPP) connect the crystalline and amorphous phases. The temperature and strain-rate dependences of the yield stress arise from the activation of these LPP, both with opposed effects. An increase on the temperature or a reduction on the strain-rate reduces the number of LPP, increasing the lamellar span and the lamellar cluster thickness, reducing σ_y. Conversely, a decrease on the temperature or an increment on the strain-rate raises the number of LPP, decreasing the lamellar span and thickening the lamellar cluster, increasing σ_y. The deformation mechanisms are explained by an elastic-beam analogue under flexural and shear loadings. The shish–kebab structure of the skin layer is more prone to a shear deformation showing a higher σ_y, whereas in the spherulitic core the lamella are more subjected to (axial) flexural loading, presenting a lower σ_y. σ_y of injection molded specimens is therefore determined by four main morphological parameters: the skin ratio, the level of molecular orientation, the lamellar (cluster) thickness and the distance between LPP. These latter are also both governed by the conformational state of the amorphous regions, and they are dependent upon the strain-rate and temperature.

Acknowledgements

This work was financially supported by FCT—Foundation for Science and Technology, through the POCTI and FEDER programmes.

References

[1] Zaroulis JS, Boyce MC. Polymer 1997;38:1303.
[2] Liu Y, Truss RW. J Appl Polym Sci, Part B: Polym Phys 1994;32:2037.
[3] Hughes DJ, Mahendrasingam A, Oatway WB, Heeley EL, Martin C, Fuller W. Polymer 1997;38:6427.
[4] Buckley C, Costas M. J Polym Sci, Part B: Polym Phys 2004;42:2081.
[5] Peterlin AJ. Mater Sci 1971;6:61.
[6] Liu Y, Kennard CHL, Truss RW, Calos NJ. Polymer 1997;38:2797.
[7] Ferreiro V, Coulon G. J Polym Sci, Part B: Polym Phys 2004;42:687.
[8] Raults J. J Mater Sci, Rev Macromol Chem Phys 1997;C37(2):335.
[9] Nitta K, Takayanagi M. J Polym Sci, Part B: Polym Phys 2000;38:1037.
[10] Takayanagi M, Nitta K, Kojima O. J. Macromol Sci, Part B: Phys 2003; B42(5):1049.
[11] Men Y, Rieger J, Strobl G. Phys Rev Lett 2003;91:9.
[12] Al-Hussein M, Strobl G. Macromolecules 2002;35:8515.
[13] Men Y, Strobl G. J Macromol Sci, Phys 2001;40:775.
[14] Graham JT, Alamo R, Mandelkern L. J Polym Sci 1997;35(2):213.
[15] Lin L, Argon AS. J Mater Sci 1994;29:294.
[16] Galeski A. Progr Polym Sci 2003;28:1643.
[17] Lim JY, Donahue HJ, Kim SY. Macromol Chem Phys 2003;204:653.
[18] Karttunen NR, Lesser AJ. Polym Eng Sci 2000;40:2317.
[19] Roetling JA. Polymer 1965;6:311.
[20] Kennedy MA, Peacock AJ, Failla MD, Lucas JC, Mandelkern L. Macromolecules 1995;28:1407.
[21] Brooks NWJ, Ducket RA, Ward IM. J Polym. Sci, Part B: Polym Phys 1998;36:2177.
[22] Brooks NWJ, Mukhtar M. Polymer 2000;41:1475.
[23] Ward IM, Hadley DW. Mechanical properties of solid polymers. Chichester, UK: Wiley; 2000.
[24] McGrum NG, Buckley CP, Bucknall CB. Principles of polymer engineering. Oxford, UK: Oxford Sci. Publ.; 1997.
[25] Brooks NW, Ghazali M, Duckett RA, Unwin AP, Ward IM. Polymer 1999;40:821.
[26] Polpi R, Mandelkern L. J Polym Sci, Part B: Polym Phys 1987;25:441.
[27] Lucas JC, Failla MD, Smith FL, Mandelkern L. Polym Eng Sci 1995;35: 1117.
[28] Monasse B, Haudin J-M. Colloid Polym Sci 1985;263:822.
[29] Mandelkern L, Alamo RG. In: Mark JE, editor. Physical properties of polymers handbook. New York: American Institute of Physics; 1996.
[30] Nitta K. Macromol Symp 2001;170:311.
[31] Sirotkin RO, Brooks NW. Polymer 2001;42:3791.
[32] Nitta K, Yamamoto Y. e-Polymers 2003 [no. 024, http//www.e-polymers.org].
[33] Hiss R, Hobeika S, Lynn C, Strobl G. Macromolecules 1999;32:4390.

[34] Viana JC, Ribeiro C, Dias GR. e-Polymer 2004 [no. 065, http//www.e-polymers.org].
[35] Mendoza R, Regniera G, Seilerb W, Lebrun JL. Polymer 2003;44:3363.
[36] Fujiyama M. In: Karger-Koscis J, editor. Polypropylene structure, blends and composites: structure and morphology, vol. 1. London: Chapman and Hall; 1995. p. 167–204.
[37] Zipper P, Janosi A, Wrentschur E, Geymayer W, Ingolic E, Friesenbichler W, et al. Int Polym Proc 1997;XII(2):192.
[38] Viana JC, Cunha AM, Billon N. Polymer 2002;43:4185.
[39] Viana JC. Polymer 2004;45:993.
[40] Viana JC, Cunha AM, Billon N. J Mat Sci 2001;36:4411.
[41] Viana JC, Billon N, Cunha AM. Polym Eng Sci 2004;44:1522.
[42] Schrauwen BAG, Von Breemen LCA, Spoelstra AB, Govaert LE, Peters GWM, Meijer HEH. Macromolecules 2004;37:8618.
[43] Kalay G, Bevis MJ. Plast Rubber Compos Process Appl 1995;23(2):71.
[44] Tjong SC, Shen JS, Li RKY. Polym Eng Sci 1996;36(1):100.
[45] Lim JY, Donahue HJ, Kim SY. Macromol Chem Phys 2003;204:653.
[46] Godinho JS, Cunha AM, Crawford RJ. Plast Rubber Compos Process Appl 2000;29:329.
[47] Cunha AM, Godinho JS, Viana JC. In: Cunha AM, Fakirov S, editors. Structure development during polymer processing, NATO-ASI series, vol. 370. Dordrecht (Hingham, MA): Kluver Academics Pub.; 2000. p. 255–77.
[48] Phillips R, Herbert G, News J, Wolkowicz J. Polym Eng Sci 1994;34:1731.
[49] Kech A, Ludwig H-C, Eyerer P. Proceedings of the 3rd ESAFORM conference material forming, 2000, ed. H.G. Fritz, Stuttgart, Germany, V.35 (ISBN. 3-00-005861-3).
[50] Viana JC, Cunha AM, Billon N. Polym Eng Sci 1999;39:146.
[51] Nitta K. Compos Theor Simul 1999;9:19.
[52] Hugel T, Strobl G, Thomann R. Acta Polym 1999;50:214.